



**HAL**  
open science

## Meso-scale signatures of inertial transitions in granular materials

A. Clerc, A. Wautier, Stéphane Bonelli, François Nicot

► **To cite this version:**

A. Clerc, A. Wautier, Stéphane Bonelli, François Nicot. Meso-scale signatures of inertial transitions in granular materials. *Granular Matter*, 2021, 23 (2), pp.24/28. 10.1007/s10035-021-01087-5 . hal-03184125

**HAL Id: hal-03184125**

**<https://hal.inrae.fr/hal-03184125>**

Submitted on 22 Jul 2021

**HAL** is a multi-disciplinary open access archive for the deposit and dissemination of scientific research documents, whether they are published or not. The documents may come from teaching and research institutions in France or abroad, or from public or private research centers.

L'archive ouverte pluridisciplinaire **HAL**, est destinée au dépôt et à la diffusion de documents scientifiques de niveau recherche, publiés ou non, émanant des établissements d'enseignement et de recherche français ou étrangers, des laboratoires publics ou privés.

# Meso-scale signatures of inertial transitions in granular materials

A. Clerc<sup>1\*</sup>, A. Wautier<sup>1</sup>, S. Bonelli<sup>1</sup> and F. Nicot<sup>2</sup>

<sup>1</sup> INRAE, Aix Marseille Univ., RECOVER  
3275 Rte Cézanne, CS 40061, 13182 Aix-en-Provence Cedex 5, France

<sup>2</sup> Université Grenoble Alpes, INRAE, ETNA  
2 Rue de la Papeterie BP 76, 38402 Saint Martin d'Hères, France

## Abstract

Granular materials have a complex collective behavior based on simple interactions between grains. The global behavior stems from dynamic rearrangements in the micro-structure. The local increase (resp. decrease) of the density generates jamming (resp. unjamming). In this paper, instabilities in the form of localized bursts of kinetic energy are studied at both the micro-scale (i.e. grain scale) and meso-scale (i.e. cluster scale). The bursts are defined from the variation of kinetic energy. The meso-domains (grain loops in 2D) are built from the tessellation of the medium. We analyze the gain and loss of meso-structures during a localized burst. Surprisingly, micro-structural reorganizations are able to keep the overall statistical equilibrium constant. The introduction of strain-like and stress-like quantities at the mesoscopic scale makes it possible to propose an expression that can be assimilated to mesoscopic second-order work. At this intermediate scale, the negative values of the second-order work are correlated to the appearance of bursts of kinetic energy, which stands for a meso-scale counterpart of Hill's macroscopic criterion of mechanical instability.

**Key Words:** granular materials, kinetic energy, instability, DEM, meso-scale, meso-domain

## 1 **1. Introduction**

2 Granular materials exhibit a complex behavior. A set of solid grains can behave collectively like a solid,  
3 in quasi-static regime, or like a fluid, in an inertial regime. Understanding and modeling the diversity of  
4 behavior and especially the inertial transition has been an active subject for many years (Cambou, Jean,  
5 & Radjai 2013, Forterre & Pouliquen 2008, Vescovi et al. 2018). Inertial transition has a key role to  
6 play in the triggering of natural hazards such as landslides or avalanches, or in the failure of civil  
7 engineering structures such as earth dams or levees (Wautier et al. 2018b). For such events, bursts of  
8 kinetic energy are signatures of mechanical instability and they stand for early clues of inertial  
9 transitions (Darve et al. 2004, Gaume et al. 2011, Wautier et al. 2018a). Thus, a close look at these bursts  
10 makes a lot of sense to anticipate regime changes in granular materials (Peng et al 2016, Gaume et al.  
11 2018, Marteau et al. 2018, Walker and Tordesillas 2016, Welker and McNamara 2011). Although these  
12 instabilities can have consequences at the macro-scale, they come from sources at the microscopic scale.  
13 By looking at small scales, we tend to find precursors to the bursts and identify inertial transition  
14 mechanisms. However, it should be emphasized that the constitutive features of granular materials stem  
15 from grain rearrangements and subsequent geometrical transformations. Although local behaviour  
16 dictates the mutual interaction between contacting particles, mechanisms at the mesoscopic scale are  
17 also thought to be very important. As a desire to bridge the gap between constitutive purposes at the  
18 macro-scale and elementary considerations at the micro-scale, multi-scale approaches are often  
19 considered to study granular materials (Liu et al. 2018, Nguyen et al 2009, Nguyen et al. 2012, Staron  
20 et al. 2005, Zhu 2016). Meso-structures such as force chains (Peters et al. 2005, Radjai et al. 1996,  
21 Tordesillas 2007, Wautier et al. 2017, Wautier et al. 2018b) and grain loops (Liu et al. 2018, Liu et al.  
22 2020, Zhu et al. 2016) have already proven to be relevant to give information on how forces and  
23 geometrical reorganization take place. It is also on a meso-scopic scale that experimental investigations  
24 are currently being carried out (Le Bouil et al. 2014).

25 In the context of continuum mechanics, including granular materials, instabilities depend on a  
26 strain/stress state in comparison with loading conditions. Nicot and Darve (2007) and Nicot et al. (2009,  
27 2012) have formulated a criterion resuming Hill's sufficient condition of stability (1958). For a material  
28 point and for small increments, this criterion reads as follow : "For a given equilibrium  $(\boldsymbol{\sigma}, \boldsymbol{\varepsilon})$  reached  
29 after a given loading history, the material point is unstable if there exists at least one stress increment  
30  $\Delta\boldsymbol{\sigma}$ , associated with a strain response  $\Delta\boldsymbol{\varepsilon}$  such that  $\Delta\boldsymbol{\sigma}:\Delta\boldsymbol{\varepsilon}<0$ ". For granular materials, Nicot and Darve  
31 (2007) have already derived the relationship between kinetic energy variations and the second-order  
32 work at the material point scale. In this work, the second-order work is calculated from either  
33 macroscopic (stress and strain tensors) quantities or as a summation of local terms built on microscopic  
34 quantities (contact forces and inter-granular velocities). The ability of the microscopically defined  
35 second-order work to anticipate the occurrence of micro-burst of kinetic energy has been highlighted  
36 (Darve et al. 2004, Nicot et al. 2007 and 2011, Wan et al., 2017). However, no works proposed yet a

1 meso-scale definition of the second-order work attached to physical meso-structures relevant to capture  
2 the driving elementary mechanisms giving rise to the overall behavior of granular materials.  
3 In this paper, we use meso-domains to study bursts of kinetic energy through numerical simulations  
4 based on a discrete element method (DEM) which has proved to be a relevant and powerful tool to study  
5 granular material either from a solid or a fluid like point of view (Méjean et al. 2017, Sibille et al. 2019,  
6 Nguyen et al. 2016). Grain loops are well-defined meso-structures in 2D, but their extension to the 3D  
7 case is still an open question (Nguyen et al. 2020). Therefore, DEM simulations are performed in a two-  
8 dimensional set up. Inertial transition potentials and consequences at the micro- and macro-scale are  
9 examined. The evolution of the second-order work is studied on a mesoscopic scale to link potential  
10 instability and inertial transition, which has not yet been done to our knowledge. This paper is organized  
11 as follows. In the first section, 2D biaxial tests are presented. In the second section, we analyze the  
12 evolution of kinetic energy during the biaxial test. The third section proposes a definition of the meso-  
13 structures of interest (namely grain loops), and a rationale formulation of strain and stress increments  
14 attached to them. The last section is devoted to the analysis of the results obtained in terms of meso-  
15 scale evolutions of micro-structure.

16

## 17 **2. Numerical Set Up**

18 Numerical experiments are carried out with quasi-2D numerical samples using DEM's open-source  
19 YADE code (Šmilauer et al. 2010). Quasi 2D conditions refer to planar samples composed of spheres,  
20 in comparison to the real 2D characterized by planar samples made of discs (Staron et al. 2002, Hadda  
21 et al., 2016). Although 3D simulations are possible, meso-structures are, for the moment, only well  
22 defined in two-dimensional samples by grain loops (Zhu et al. 2016, Liu et al. 2018, Liu et al. 2020,  
23 Nguyen et al. 2012). The definition of meso-domains in 3D samples is still an object of research (Nguyen  
24 et al. 2020) and is out of the scope of this paper.

25 An idealized granular sample consisting of 25,000 spheres in interaction through an elasto-frictional  
26 contact law is considered in this paper (Figure 1a). The particle radii are uniformly distributed with a  
27 size ratio  $D_{max}/D_{min}$  of 3.5. All sample parameters are recalled in Table 1. The spheres are placed  
28 randomly in a square domain which allows working at the material point scale, i.e. at a scale where it is  
29 possible to obtain both global (continuum) and local (discrete) views of the granular medium. In order  
30 to create a dense sample, the friction coefficient  $\mu$  at each contact is gradually reduced from 0.7 to 0,  
31 while maintaining a pressure of 100 kPa on the lateral boundaries in the preparation step. For a clear  
32 understanding of the procedure in quasi 2D, the third and unused dimension of the specimen has been  
33 set to one unit length, so that stresses applied on the boundaries can be expressed either in kPa or in N/m  
34 simply by dividing the sum of the contact forces by the sample length or width. Numerical damping is  
35 chosen low, so as not to inhibit the creation and propagation of kinetic energy bursts (Table 1).

1 The biaxial compression test is broken down into two phases. An isotropic compression of  $\sigma_0 = 100$  kPa  
 2 is firstly applied. The confining pressure  $\sigma_0$  is then maintained constant on the lateral boundaries while  
 3 imposing a strain rate  $\dot{\varepsilon}$  in the vertical direction (Figure 1b, Table 1).

4 The 2D expressions of the deviatoric stress  $q$  and the volumetric strain  $\varepsilon_v$  are

$$5 \quad q = \left| \sigma_{yy} - \sigma_{xx} \right| \quad , \quad \varepsilon_v = \varepsilon_{xx} + \varepsilon_{yy} \quad (1)$$

6 The  $q - \varepsilon_{yy}$  curve is typical of the response of a dense sample as shown in Figure 2, where the vertical  
 7 lines A and B represent respectively the characteristic point of the volumetric strain  $\varepsilon_v$  and the maximum  
 8 of the deviatoric stress  $q$ . The curve shows a hardening regime represented by a strong increase leading  
 9 to a peak ; then a softening regime takes place, with a small decrease of the deviatoric stress followed  
 10 by a plateau. Here the  $q$  peak is obtained at less than 1% of the axial strain (line B in Figure 2). An early  
 11  $q$  peak is often found with numerical simulations compared to experimental simulations, which is  
 12 attributed to the use of the perfect spheres in DEM instead of irregular shapes as with real particles. The  
 13  $\varepsilon_v$  curve is also characteristic of a dense material with, firstly, a small compression behavior, the  
 14 maximum of which is reached before the  $q$  peak (vertical line A in Figure 2), and secondly, a dilation  
 15 until the end of the test.

16

### 17 **3. Analysis of bursts of kinetic energy**

18 Using numerical simulation, the data can be analyzed either at the whole sample level or at the grain or  
 19 cluster scale. Figure 3 shows the changes in elastic, plastic and kinetic energies as a function of axial  
 20 strain during the biaxial test. Kinetic energy is represented with a different scale to highlight the  
 21 frequency of large variations. In Figure 3, dashed blue vertical lines highlight the occurrence of the  
 22 bursts studied in this paper given by:

$$23 \quad E_c^g = \frac{1}{2} m_g \left\| \mathbf{c}_g \right\|^2 + \frac{1}{5} m_g \left| \omega R_g \right|^2 \quad (2)$$

24 where  $m_g$  is the grain mass,  $R_g$  is the grain radius,  $\mathbf{c}_g$  and  $\omega_g$  are the translation velocity vector and the  
 25 rotation velocity of the grain, respectively.

26 For elasto-frictional contacts (Figure 1a), the stored elastic energy of a contact is

$$27 \quad E_e^c = \frac{1}{2} k_n (u_n^c)^2 + \frac{1}{2} k_t \left\| \mathbf{u}_t^c \right\|^2 = \frac{1}{2} k_n^{-1} (F_n^c)^2 + \frac{1}{2} k_t^{-1} \left\| \mathbf{F}_t^c \right\|^2 \quad (3)$$

28 where  $k_n$  and  $k_t$  are the normal and tangential stiffnesses,  $u_n^c$  and  $\mathbf{u}_t^c$  the normal and tangential relative  
 29 displacements at contact,  $F_n^c$  and  $\mathbf{F}_t^c$  are the normal and tangential contact forces.

30 When contact sliding occurs ( $\left\| \mathbf{F}_t^c \right\| = \mu F_n^c$ ), some energy is dissipated. A non-reversible tangential  
 31 displacement velocity  $\dot{\mathbf{u}}_t^c$  generates a positive plastic dissipation

$$32 \quad \dot{E}_p^c = \mathbf{F}_t^c \cdot \dot{\mathbf{u}}_t^c \quad (4)$$

1 From the Eqs. (2)-(4), energy variations at the sample scale during the deviatoric loading over a given  
 2 time range  $[t_0, t]$  are obtained by summing the kinetic energy  $E_c$  on the grains, and by summing the  
 3 elastic energy  $E_e$  and the plastic dissipation  $E_p$  on the contacts:

$$4 \quad \Delta E_c(t) = \sum_g E_c^g(t) - E_c^g(t_0) \quad , \quad \Delta E_e(t) = \sum_c E_e^c(t) - E_e^c(t_0) \quad , \quad \Delta E_p(t) = \int_{t_0}^t \sum_c \dot{E}_e^c(t') dt' \quad (5)$$

5 Local outbursts of kinetic energy are detected if the kinetic energy of a part of the sample is greater than  
 6 the mean kinetic energy. The overall kinetic energy of the sample is of the order of  $10^{-8}$  J. The mean  
 7 kinetic energy of a grain (out of 25,000) is therefore of the order of  $10^{-13}$  J. As shown in Figure 3, there  
 8 are many important variations from the mean value. Four bursts of kinetic energy are chosen and studied  
 9 (Figure 4). They occur on the  $q$  plateau (Figure 4a) where a quasi-stationary regime corresponding to  
 10 the so-called ‘critical state’ is reached (state at which a granular material can be continuously sheared  
 11 under a constant mean pressure without any change in volume). A close look on the deviatoric stress  
 12 curve around the appearance of the bursts is provided in Figures 4b, 4c and 4d. This highlights the fact  
 13 that the onset of each burst corresponds to a drop in  $q$ . A localized explosion of kinetic energy has thus  
 14 some macroscopic consequences in the form of a small transient instability. Burst No.2 and No.3 were  
 15 initially detected as a single burst, but after a more detailed examination, they appeared to be two  
 16 consecutive bursts that propagate in slightly different areas.

17 For the sake of clarity, only burst No.4 is investigated in the following. All the presented results are  
 18 similar for other bursts. Figure 5 shows a reduced time lapse for the burst 4. It highlights the typical  
 19 onset and evolution of kinetic bursts of energy observed on the constant  $q$  plateau of a drained biaxial  
 20 test. In Figure 5, grains that have a kinetic energy at least twice the mean kinetic energy of a grain are  
 21 highlighted. From a state where most grains have a low kinetic energy (less than the mean kinetic energy  
 22 of a grain), the initiation affects only a few grains, before spreading to nearly half of the sample and  
 23 disappearing. In its initiation, propagation and attenuation, the center of the burst moves slightly in the  
 24 positive direction of x-axis, but the set of grains with large kinetic energy remains limited and the burst  
 25 does not propagate to the whole sample, as it could be observed in case of material instability (Wautier  
 26 et al. 2018a).

27 To better understand the mechanisms that trigger a burst and drive its propagation, we need to  
 28 distinguish the area where the burst occurs and propagates from the rest of the sample domain. This is  
 29 done with use of a fixed box defined around the burst, considering the location of the start and the  
 30 direction of propagation (Figure 5c). On the Figure 5c, the box is displayed, showing a rectangle of  
 31 dimensions  $[0.03 \text{ m}, 0.032 \text{ m}]$  centered on the point  $(0.045 \text{ m}, 0.046 \text{ m})$ . The same energy variation  
 32 analysis as in Figure 3 at the scale of the defined box is reported in Figure 6. The energy variations show  
 33 that, when the kinetic energy breaks up (vertical lines), the kinetic energy passes through a peak, while  
 34 the elastic energy decreases, and the plastic energy increases (Figure 6). On the basis of these variations,  
 35 it is concluded that there is an excess of elastic energy stored in the contacts, which is then transformed

1 into kinetic energy (the grains move linearly or rotate) and dissipated by friction (corresponding to a  
2 slip between the grains in the contacts). However, the variations in kinetic energy are very small  
3 compared with the variations in plastic energy. Frictional dissipation is thus the main mechanism active  
4 during the burst of kinetic energy. Kinetic energy, which is the easiest signature of local instabilities,  
5 represents indeed only a small part of the energy transfer from the elastic energy for kinetic outbursts  
6 occurring at critical state in drained biaxial tests. It should be underlined that this analysis depends on  
7 the contact friction. In the two extreme cases of frictionless grains ( $\mu = 0$ ) or fully elastic contacts ( $\mu =$   
8  $+\infty$ ), no plastic dissipation can occur, and the elastic energy transforms entirely into kinetic energy.  
9 However, for intermediate friction (corresponding to more realistic materials), and for similar stress  
10 levels, the above analysis holds with dissipative mechanisms being prominent.  
11 These energetic considerations are only a first step towards understanding the origins of bursts.  
12 Additional parameters are required to investigate the location of the burst in a specific area. The sliding  
13 index  $I_p$  for each contact is defined as follows:

$$14 \quad I_p = \frac{\|\mathbf{F}_t\|}{\mu |F_n|} \quad (6)$$

15 This index, belonging to the [0,1] interval, is an indicator of the potential instability of a contact (the  
16 value 1 corresponding to contact sliding). The probability density of  $I_p$  for contacts inside and outside  
17 the kinetic energy burst zone is given in Figure 7. Before the burst, a larger fraction of the contacts is  
18 close to sliding ( $I_p$  close to 1) in the burst domain than outside. After the occurrence of the burst (Figure  
19 7), no unstable contacts remain in the burst domain (the tail of the  $I_p$  probability density function inside  
20 the burst domain converges to the one out of the burst domain). The probability curve outside the zone  
21 does not change much.  $I_p$  close to 1 is a necessary condition to observe a burst of kinetic energy. Similar  
22 findings were obtained by Wautier et al. (2018a).

23 This last result reinforces the delineation of the burst zone and provides clues to relate the burst spatial  
24 extension to some underlying microstructure characteristics. There is a strong contrast between the  
25 behavior of grains inside and outside of the area. The burst is likely to be rooted in a zone with high  
26 level of stored elastic energy and high concentration of unstable contacts. The analysis will now be  
27 carried out on a mesoscopic scale, which requires the definition of relevant mechanical quantities at this  
28 scale.

29

## 30 **4. Definition of quantities at the mesoscopic scale**

### 31 *4.1. Definition of meso-domains*

32 In order to define clusters of grains, a convenient method in 2D is to tessellate the sample area with grain  
33 loops. As a result, the sample domain can be seen as the union of loops involving a variable number of  
34 grains. Recent studies have shown the relevance of defining such a meso-scale based on grain loops to

1 characterize changes in the micro-structure of granular materials (Nguyen et al. 2012, Zhu et al. 2016,  
2 Liu et al. 2018).

3 A unique tessellation is obtained, with loops of order 3, 4, 5 and 6+ according to the number of spheres  
4 they contain (Figure 8 show a small portion of the tessellation). The loop porosity is expected to increase  
5 with the loop order. Thus, lower order loops are on average less deformable than higher order loops.  
6 Grain loops play a key role in the reorganization of the micro-structure, as a means of adapting to  
7 external loadings. Non-contact or single-contact grains, called rattlers, are visible inside the high-order  
8 loops in Figure 8. They are also good indicators of reorganization since they are created from broken  
9 meso-structures and they can be trapped in meso-structures under construction.

10

#### 11 4.2. Definition of a mesoscopic second-order work

12 The ability of a system to develop kinetic energy with no external disturbance from an equilibrium state<sup>1</sup>  
13 is described by the balance equation of second-order works

$$14 \quad 2E_c(t + \Delta t) = W_2^{ext} - W_2^{int} \quad (7)$$

$$15 \quad W_2^{ext} = \int_{\partial\Omega} \Delta \mathbf{f} \cdot \Delta \mathbf{u} dA \quad , \quad W_2^{int} = \int_{\Omega} \Delta \boldsymbol{\sigma} : \Delta \boldsymbol{\varepsilon} dV \quad (8)$$

16 where  $E_c$  represents the overall kinetic energy,  $W_2^{ext}$  is the external second-order work,  $W_2^{int}$  is the  
17 internal second-order work,  $\mathbf{f} = \boldsymbol{\sigma} \cdot \mathbf{n}$  and  $\mathbf{u}$  denote the stress and displacement vectors on  $\partial\Omega$ ,  $\boldsymbol{\sigma}$  and  $\boldsymbol{\varepsilon}$   
18 denote the stress and strain tensors in  $\Omega$ , and  $\Delta$  is the increment between times  $t$  and  $t + \Delta t$ .

19 There are two requirements for using second-order work criteria for a stability analysis:

20 - this criterion is most often used when the system control parameters are kept constant, or  $\Delta \mathbf{f} \cdot \Delta \mathbf{u} = 0$  on  
21  $\partial\Omega$ , to highlight situations where the deformation of the system can be carried on without any input of  
22 external energy;

23 - the system must be in balance initially ( $E_c(t) = 0$ ). As  $W_2^{ext} = 0$ , the system evolves from a static  
24 situation to a inertial regime ( $E_c(t + \Delta t) > 0$ ) is only if  $W_2^{int} < 0$ . Therefore, Eq. (8) does not apply  
25 once the system is out of equilibrium.

26 There is a priori no reason for the selected meso-domains to check these two conditions. Despite these  
27 restrictions, we propose to define adequate quantities  $\langle \boldsymbol{\sigma} \rangle_{\Omega_l}$  and  $\langle \boldsymbol{\varepsilon} \rangle_{\Omega_l}$ , corresponding to stresses and  
28 strains in a mesoscopic domain  $\Omega_l(t)$ , and to analyze the evolution of a so-called mesoscopic second-  
29 order work

$$30 \quad (W_2)_{\Omega_l} = \langle \Delta \boldsymbol{\sigma} \rangle_{\Omega_l} : \langle \Delta \boldsymbol{\varepsilon} \rangle_{\Omega_l} \quad (9)$$

31 This approach assumes that the Macro-Homogeneity condition (second-order Hill-Mandel lemma) is  
32 respected on the domain  $\Omega$ :

---

<sup>1</sup> An equilibrium state is characterized by a nil kinetic energy, and by the fact that any variation of energy from the current state is a second order function of the applied perturbation.



$$\langle \Delta \boldsymbol{\sigma} : \Delta \boldsymbol{\varepsilon} \rangle_{\Omega} = \langle \Delta \boldsymbol{\sigma} \rangle_{\Omega} : \langle \Delta \boldsymbol{\varepsilon} \rangle_{\Omega} \quad , \quad \langle \bullet \rangle_{\Omega} = \frac{1}{|\Omega|} \int_{\Omega} \bullet dV \quad (10)$$

The necessary conditions to ensure the validity of this second-order Hill-Mandel lemma has been discussed in details in Nicot et al. (2017). Such a relationship has not yet been discussed for mesoscopic quantities, for which the domain  $\Omega$  cannot be considered as a representative elementary volume. Therefore, the specific form of equation (7) at the mesoscale remains to be discussed. Such an analytical discussion is saved for future investigations as it is out of the scope of the present paper.

#### 4.3. Definition of the mesoscopic incremental strain

The average strain rate  $\langle \boldsymbol{\varepsilon} \rangle_{\Omega_l}$  on a domain  $\Omega_l$  is completely defined in terms of quantities on the boundary  $\partial\Omega_l$  as follows:

$$\langle \boldsymbol{\varepsilon} \rangle_{\Omega_l} = \frac{1}{|\Omega_l|} \int_{\partial\Omega_l} \mathbf{u} \otimes_s \mathbf{n} dA \quad (11)$$

where  $\mathbf{u}$  is the displacement vector,  $\mathbf{n}$  is the outer normal to  $\Omega_l$ , and  $\otimes_s$  denotes the symmetric tensor product ( $\mathbf{u} \otimes_s \mathbf{n} = \frac{1}{2}(\mathbf{u} \otimes \mathbf{n} + \mathbf{n} \otimes \mathbf{u})$ ). The analysis of kinetic energy at the microscopic scale is carried out in very small-time steps  $\Delta t$ . It is therefore relevant to assume that the system undergoes small perturbations between  $\Omega_l(t)$ , and  $\Omega_l(t + \Delta t)$ . This point is debatable though and will have to be considered by further research.

The incremental meso-strain between time  $t$  and  $t + \Delta t$  can be expressed by means of the incremental displacement vector  $\Delta \mathbf{u} = \mathbf{u}(t + \Delta t) - \mathbf{u}(t)$ :

$$\langle \Delta \boldsymbol{\varepsilon} \rangle_{\Omega_l} = \frac{1}{|\Omega_l|} \int_{\partial\Omega_l} \Delta \mathbf{u} \otimes_s \mathbf{n} dA \quad (12)$$

where  $\Omega_l$  and  $\mathbf{n}$  are considered at time  $t$ . As the domain  $\Omega_l$  is updated at each increment, it is an updated Lagrangian description which allows large strains at the mesoscopic level over a large number of time steps.

A grain loop is delimited by branch vectors joining the center of neighbor spheres (Figure 9a). This is the polygon on which the meso-strain calculations are based. The meso-strain tensor as a grain loop quantity can be expressed as a function of a linear interpolation of the incremental displacements of the peripheral grains (Nguyen et al. 2012, Bonelli et al. 2012):

$$\langle \Delta \boldsymbol{\varepsilon} \rangle_{\Omega_l} = \frac{1}{|\Omega_l|} \sum_{k \in \partial\Omega_l} \frac{1}{2} (\Delta \mathbf{u}_k^0 + \Delta \mathbf{u}_k^1) \otimes_s \mathbf{n}_k l_k \quad (13)$$

where  $\mathbf{u}_k^0$  and  $\mathbf{u}_k^1$  are the incremental displacement vectors of the vertices of the  $k^{\text{th}}$  edge (grains centers),  $l_k$  is the length of the  $k^{\text{th}}$  edge, and  $\mathbf{n}_k$  is the normal to the  $k^{\text{th}}$  edge (outer to  $\Omega_l$ ).

#### 4.4. Definition of the mesoscopic incremental stress

1 For the stress tensor, deriving an incremental formulation is more complex than it might appear at first  
 2 glance. Indeed, defining a meso-stress is relatively simple with use of Love-Weber or Bagi formulas  
 3 (Bonelli et al., 2012, Nicot et al., 2013, Yan et al., 2019), but an incremental formulation requires that  
 4 the loops are not reorganized between two close configurations. To address this issue, we are looking  
 5 for a definition of incremental meso-stress based on the incremental stresses in the grains. The meso-  
 6 stress is expressed as the spatial average on  $\Omega_l$  of the micro-stress (Figure 9b):

$$7 \quad \langle \boldsymbol{\sigma} \rangle_{\Omega_l} = \frac{1}{|\Omega_l|} \int_{\Omega_l} \boldsymbol{\sigma} dV \quad (14)$$

8 As the local stress tensor  $\boldsymbol{\sigma}$  is equal to zero in empty space, the integral can be transformed into a sum  
 9 over the portions of the spheres included in  $\Omega_l$ , noted  $V_g \cap \Omega_l$ :

$$10 \quad \langle \boldsymbol{\sigma} \rangle_{\Omega_l} = \frac{1}{|\Omega_l|} \sum_{g \in \partial \Omega_l} \int_{V_g \cap \Omega_l} \boldsymbol{\sigma} dV \quad (15)$$

11 By introducing the average stress on the parts of the spheres included in  $\Omega_l$ , noted  $\langle \boldsymbol{\sigma} \rangle_{V_g \cap \Omega_l}$ , it comes

$$12 \quad \langle \boldsymbol{\sigma} \rangle_{\Omega_l} = \frac{1}{|\Omega_l|} \sum_{g \in \partial \Omega_l} |V_g \cap \Omega_l| \langle \boldsymbol{\sigma} \rangle_{V_g \cap \Omega_l} \quad (16)$$

13 In addition, if the average stress calculated on the part of the spheres included in the loop is assumed to  
 14 be equal to the average stress of the grain:  $\langle \boldsymbol{\sigma} \rangle_{V_g \cap \Omega_l} = \langle \boldsymbol{\sigma} \rangle_{V_g}$ , the meso-stress is then proportional to the  
 15 sum of the grains stress weighted by their volume fraction in  $\Omega_l$  (Figure 9b):

$$16 \quad \langle \boldsymbol{\sigma} \rangle_{\Omega_l} = \frac{1}{|\Omega_l|} \sum_{g \in \partial \Omega_l} |V_g \cap \Omega_l| \langle \boldsymbol{\sigma} \rangle_{V_g} \quad (17)$$

17 Although the grains are assumed rigid in DEM, they are subject to a local stress  $\boldsymbol{\sigma}$ , which is a  
 18 symmetrical second-order tensor and verifies the equation of motion  $\rho \ddot{\mathbf{x}} = \text{div}(\boldsymbol{\sigma})$  and  $\boldsymbol{\sigma} = \boldsymbol{\sigma}^T$ . Thus,  
 19 in dynamic evolution, the average stress  $\langle \boldsymbol{\sigma} \rangle_{V_g}$  is equal to

$$20 \quad \langle \boldsymbol{\sigma} \rangle_{V_g} = \frac{1}{|V_g|} \int_{\partial V_g} \boldsymbol{\sigma} \cdot \mathbf{n} \otimes_s (\mathbf{x} - \mathbf{c}_g) dA + \frac{1}{|V_g|} \int_{V_g} \rho \ddot{\mathbf{x}} \otimes_s (\mathbf{x} - \mathbf{c}_g) dV \quad (18)$$

21 The grain is only subjected to punctual contact forces vectors  $\mathbf{f}_c$  on  $\partial V_g$ , therefore, the left-hand side  
 22 term of Eq. (18) is equal to

$$23 \quad \frac{1}{|V_g|} \int_{\partial V_g} \boldsymbol{\sigma} \cdot \mathbf{n} \otimes_s (\mathbf{x} - \mathbf{c}_g) dA = \frac{D_g}{2|V_g|} \sum_{c \in \partial V_g} \mathbf{f}_c \otimes_s \mathbf{n}_c \quad (19)$$

24 where the index  $c$  runs through all contacts of the grain  $g$ ,  $D_g$  is the grain diameter, and  $\mathbf{n}_c$  is the outer  
 25 normal to  $V_g$  at contact  $c$ .

26 The kinematics of the rigid grain is described by  $\dot{\mathbf{x}} = \dot{\mathbf{c}}_g + \mathbf{Q}_g \cdot (\mathbf{x} - \mathbf{c}_g)$  for any  $\mathbf{x} \in V_g$ , where  $\mathbf{c}_g$  is the  
 27 grain center, and  $\mathbf{Q}_g$  is the second-order skew-symmetric tensor describing the grain rotation. Therefore,  
 28 the second right-hand side term of Eq. (19) is equal to

$$\frac{1}{|V_g|} \int_{V_g} \rho \ddot{\mathbf{x}} \otimes_s (\mathbf{x} - \mathbf{c}_g) dV = \frac{\rho D_g^2}{10} (\dot{\mathbf{Q}}_g + \mathbf{Q}_g^2) \quad (20)$$

as  $\ddot{\mathbf{x}} = \ddot{\mathbf{c}}_g + (\dot{\mathbf{Q}}_g + \mathbf{Q}_g^2) \cdot (\mathbf{x} - \mathbf{c}_g)$ . It is assumed here that the contribution of grain rotation is negligible compared to the contribution of contact forces. This is justified by the fact that the ratio between rotation term Eq. (20) and contact force term Eq. (19) scales with  $D_g^4$ . Nevertheless, since contact forces are likely to become very weak during a burst of kinetic energy, this point is debatable and will have to be verified by further research.

Finally, the expression of the meso-stress is of a form similar to, but different from the Love-Weber formula for the set of grains concerned:

$$\langle \boldsymbol{\sigma} \rangle_{\Omega_l} = \frac{1}{|\Omega_l|} \sum_{g \in \partial \Omega_l} \frac{D_g |V_g \cap \Omega_l|}{2|V_g|} \sum_{c \in \partial V_g} \mathbf{f}_c \otimes_s \mathbf{n}_c \quad (21)$$

This difference is due to the fact that the domain  $\Omega_l$  is defined by the centers of the grains and does not contain the entire volume of grains. This definition is similar but not identical to that of Liu et al (2020). Moreover, this expression is not restricted to a quasi-static evolution and can be extended to dynamical situations when the contribution of rotations given by Eq. (20) is non-negligible. Note that Eq. (18) is consistent with the macro-stress definition computed at the scale of the sample  $\Omega$ :

$$\langle \boldsymbol{\sigma} \rangle_{\Omega} = \frac{1}{|\Omega|} \int_{\Omega} \boldsymbol{\sigma} dV = \frac{1}{|\Omega_l|} \sum_{g \in \partial \Omega} |V_g| \langle \boldsymbol{\sigma} \rangle_{V_g} = \frac{1}{|\Omega_l|} \sum_l \sum_{g \in \partial \Omega_l} |V_g \cap \Omega_l| \langle \boldsymbol{\sigma} \rangle_{V_g} = \frac{1}{|\Omega_l|} \sum_l |\Omega_l| \langle \boldsymbol{\sigma} \rangle_{\Omega_l} \quad (22)$$

The hypothesis of small geometric transformations between times  $t$  and  $t+\Delta t$  allows to suppose that

$$\langle \Delta \boldsymbol{\sigma} \rangle_{\Omega_l} = \Delta \langle \boldsymbol{\sigma} \rangle_{\Omega_l} \quad (23)$$

Thus, the incremental meso-stress between time  $t$  and  $t+\Delta t$  is now simply defined as follows

$$\langle \Delta \boldsymbol{\sigma} \rangle_{\Omega_l} = \langle \boldsymbol{\sigma}(t + \Delta t) \rangle_{\Omega_l} - \langle \boldsymbol{\sigma}(t) \rangle_{\Omega_l} \quad (24)$$

where  $\Omega_l$  is considered at time  $t$ . As the domain  $\Omega_l$  is updated at each increment, it is an updated Lagrangian description.

## 5. Analysis of the changes at the mesoscopic scale during the outburst of kinetic energy

### 5.1. Evolution of meso-structures during the burst of kinetic energy

The ratio of each loop category (L3, L4, L5, L6+) depends on the nature of the sample and the loading history. In Figure 10, the evolution of the loop ratios along a biaxial test is given against the volumetric strain. Before maximum contractancy (vertical line A in figure 4), low order loops are the majority (about 70% of loops of order 3 and 4), and loops of order 6 or higher are the minority (between 10 and 15% of the total fraction of the loop). However, from the maximum deviatoric stress state (vertical line B in Figure 4), loops of order higher than 6 are more numerous than those of lower order, while the fraction of loops of order 5 remains stable. Referring to Liu et al. (2018), two distinct evolutions can be

1 envisaged for dense sample when a strain localization develops. In the present biaxial test, no strain  
2 localization is observed. As a result, it is observed that the final proportion of loops found in at the  
3 steady-state are very similar to those reported in Liu et al. (2018) when restricting the analysis to the  
4 shear band domain only. With the help of Figure 2, we can also interpret this evolution from less  
5 deformable loops to more deformable loops as a mesoscopic equivalent of the macro-evolution of the  
6 volumetric strain: the appearance of the dilatancy goes hand in hand with the increase of the fraction of  
7 loops that contain more void.

8 The evolution rate of grain loops and rattlers are now studied during the burst of kinetic energy, inside  
9 and outside the burst zone. The relative evolution of the number of loops is equal to  $\frac{N_t}{N_0} - 1$  where  $N_t$  is  
10 the number of loops at time  $t$ . Figure 11 shows the concentration of the changes within the burst zone,  
11 even if small reorganizations persist after the burst. Figure 11a shows the rate of change of the 4 main  
12 orders of loops, within the burst area. There is about the same amount of loops created and lost for each  
13 type of loop. This means there are reorganizations of the contacts, but the mesoscopic structure remains  
14 stable on average and regains a similar structure after bursting (note that the contact force distribution  
15 is modified with less contacts close to sliding). However, we can note that the 3, 4 and 5 order grain  
16 loops are broken first (peak of lost loops in the first part of the burst) and then created (peak of gained  
17 loops in the second part of the burst). This is not obvious for 6+ order loops, which are the most affected  
18 meso-structures. Thus, low order loops are lost and transformed in higher-order loops, while higher-  
19 order loops are constantly being created and destroyed to ensure the stability of the sample during an  
20 inertial disturbance. Figure 11b shows the evolution of the proportions of new and disappeared rattlers  
21 within the bursting zone in relation to the number of rattlers just before the start of the burst. The  
22 maximum numbers of gained and lost rattlers are not reached simultaneously. This means that the  
23 rattlers are first generated and then lost. This finding is in line with the results obtained with grain loops.  
24 Before the peak of kinetic energy, a significant amount of low order loops are lost, which creates rattlers.  
25 While kinetic energy decreases, lower-order loops are created by capturing the rattlers. The loss of lower  
26 order loops in the first part of the burst (i.e. loops containing little void) is consistent with the existence  
27 of local dilatation as raised in Section III.2 and Figure 6.

28 Outside the burst zone, no significant trends can be highlighted (Figure 12). Neither grain loops (Figure  
29 12a) nor rattlers (Figure 12b) outside the burst zone are altered in number and nature. Figure 12 shows  
30 that the location of changes in micro-structures depends on the spatial location of the kinetic energy  
31 burst.

32 Identifying changes at the microscopic scale remains a difficult task, especially since the micro-structure  
33 changes are limited and concern a very small fraction of all loops. These limited changes are most likely  
34 related to the fact that, in this dense set of grains subjected to a drained biaxial compression, most of the  
35 energy is dissipated by friction rather than kinetic energy. However, the meso-domains have made it

1 possible to evidence the changes occurring in the burst zone. Grain loops highlight the microscopic  
 2 reorganization undergone by the area due to bursting.

### 4 *5.2. Analysis of the meso-stress*

5 In Figure 13, each component of the macroscopic stress is compared to the corresponding component  
 6 of the weighted average sum of all meso-stresses (the loop contributes for its fraction area of the total  
 7 sample domain). The comparison is made on the whole sample domain and on all the biaxial test long.  
 8 The dotted lines represent the components of the sum of the meso-stress. They follow very well the  
 9 evolution of each corresponding macro-component. The proposed definition of a meso-stress is thus  
 10 sound as it corresponds to the usual macroscopic definition of a stress when weighted average of the  
 11 meso-stresses is considered.

### 13 *5.3. Evolution of mesoscopic second-order work during the kinetic energy burst*

14 Figure 14 shows the spatial distribution of mesoscopic second-order works during the propagation of  
 15 the No. 4 kinetic energy burst. Meso-stress and meso-strain increments are defined on macroscopic  
 16 increments of axial strain  $|\Delta\varepsilon_{yy}| = 10^{-6}$ . Thus, each panel in Figure 14 leads to the same panel of index  
 17 in Figure 5, with the exception of the panel (\*). The vanishing of mesoscopic second-order work follows  
 18 the spatial evolution of kinetic energy, with even wider and more detailed limits. Mesoscopic second-  
 19 order work reveals some details that cannot be seen simply by looking at kinetic energy. For example,  
 20 the panel (\*) in Figure 13 is an intermediate step between (a) and (b). In Figure 5, it can be suggested  
 21 that the burst appears at the upper center of the sample. However, the panel (\*) shows that the instability  
 22 originates from the lower right corner and propagates to the upper center of the sample. The origin of  
 23 the burst at the lower right corner is also visible in panel (b) of Figure 14, but to a lesser extent.

24 Although maps of second order mesoscopic work seem to reveal more clearly the origins of the kinetic  
 25 burst, one thing to emphasize is that the whole burst area does not only have loops with negative second  
 26 order mesoscopic work. Negative and positive mesoscopic second-order loops are often next to each  
 27 other. By looking at the volume-weighted average second order work, one can assess the predominance  
 28 of negative or positive mesoscopic second order work. For the bounding box of the domain  $\Omega_b$  shown  
 29 in Figure 5, the volume-weighted average of the second-order work reads

$$30 \quad \langle W_2 \rangle_{\Omega_b} = \frac{1}{|\Omega_b|} \sum_t |\Omega_t| \langle W_2 \rangle_{\Omega_t} \quad (25)$$

31 The evolution of  $\langle W_2 \rangle_{\Omega_b}$  during the outburst of kinetic energy is shown in Figure 15.  $\langle W_2 \rangle_{\Omega_b}$  is negative  
 32 only at the nucleation of the burst. It then increases to positive values during the burst and then returns  
 33 to its pre-burst value. The decrease of  $\langle W_2 \rangle_{\Omega_b}$  prior to bursting can be seen as a signature of underlying  
 34 mechanical instability in the bursting domain. The following increase shows that the active  
 35 reorganizations of the micro-structure that occur during the burst allow for rapid restabilization of the  
 36 sample and prevent the burst from continuing to grow. As a result, the burst quickly disappears and

1 remains localized. On the other hand, it has been shown by Wautier et al. (2018a) that bursts propagating  
2 throughout the sample domain are related to mechanical instabilities at the material point scale.  
3

1  
2  
3  
4  
5  
6  
7  
8  
9  
10  
11  
12  
13  
14  
15  
16  
17  
18  
19  
20  
21  
22  
23  
24  
25  
26  
27  
28  
29  
30  
31  
32  
33  
34  
35  
36  
37

## 6. Conclusion

In this paper, we have emphasized the importance of meso-domains in the analysis of a burst of kinetic energy that can be observed in granular materials. Changes in grain loop highlight structural displacements at the microscopic scale during bursts. The opening and closing of the grain loops release kinetic energy, while the micro-structure after bursting is very similar to that before, which ensures the statistical equilibrium at critical states. Furthermore, focusing on indicators of inertial transition and mechanical instabilities, we show that the area where the burst occurred contains precursors of kinetic energy release. On the one hand, a large number of contacts with a sliding index close to 1 is required to enable the burst to be triggered in a specific area. On the other hand, the criterion of the second-order work, defined at the mesoscopic scale, predicts the burst of kinetic energy and even gives information on its origins. These results encourage the further use of meso-domains in the study of instabilities. From a more theoretical point of view, the proposed introduction of a mesoscale attached to meso-structures is based on a number of assumptions that will need to be further investigated to assess their validity where inertial terms could have a larger contribution.

## References

- Bonelli, S., Millet, O., Nicot, F., Rahmoun, D., De Saxcé G.: On the definition of an average strain tensor for two-dimensional granular material assemblies, *Int. J. Solids Struct.*, **49**, 947-958 (2012)
- Cambou, B., Jean, M., Radjaï, F. (Eds.): *Micromechanics of granular materials*. John Wiley & Sons (2013)
- Cambou, J., Magoariéc, H., Nguyen, N.-S.: *Granular Materials at the Meso-scale*. ISTE Press – Elsevier (2016)
- Darve, F., Servant, G., Laouafa, F., Khoa, H. D. V.: Failure in geomaterials: continuous and discrete analyses. *Computer methods in applied mechanics and engineering*, **193**(27-29), 3057-3085 (2004)
- Darve, F., Sibille, L., Daouadji, A., Nicot, F.: Bifurcations in granular media: macro-and micro-mechanics approaches. *C. R. Méc.*, **335**(9-10), 496-515 (2007)
- Forterre, Y., Pouliquen, O.: Flows of dense granular media. *Annu. Rev. Fluid Mech.*, **40**, 1-24 (2008)
- Gaume, J., Chambon, G., Naaim, M.: Quasistatic to inertial transition in granular materials and the role of fluctuations. *Physical Review E*, **84**(5), 051304 (2011)
- Gaume, J., Gast, T., Teran, J., van Herwijnen, A., Jiang, C.: Dynamic anticrack propagation in snow. *Nature Communications*, **9**(1), 1-10 (2018)
- Hadda, N., Sibille, L., Nicot, F., Wan, R., Darve, F.: Failure in granular media from an energy viewpoint. *Granul. Matter*, **18**(50) (2016)
- Le Bouil, A., Amon, A., Sangleboeuf, J.-C., Orain, H., Bésuelle, P., Viggiani, G., Chasle, P., Crassous, J.: A biaxial apparatus for the study of heterogeneous and intermittent strains in granular materials. *Granul. Matter*, **16**, 1–8 (2014)

- 1 Liu, J., Nicot, F., Zhou, W.: Sustainability of internal structures during shear band forming in 2D granular  
2 materials. *Powder Technology*, **338**, 458-470 (2018)
- 3 Liu, J., Wautier, A., Bonelli, S., Nicot, F., Darve, F.: Macroscopic softening in granular materials from  
4 a meso-scale perspective. *Int. J. Solids Struct.*, **193–194**, 222–238 (2020)
- 5 Nicot, F., Darve, F.: A micro-mechanical investigation of bifurcation in granular materials. *Int. J. Solids  
6 Struct.*, **44**(20), 6630-6652 (2007)
- 7 Nicot, F., Sibille, L., Darve, F.: Bifurcation in granular materials: An attempt for a unified framework.  
8 *Int. J. Solids Struct.*, **46**(22-23), 3938-3947 (2009)
- 9 Nicot, F., Sibille, L., Darve, F.: Failure in rate-independent granular materials as a bifurcation toward a  
10 dynamic regime, *International Journal of Plasticity*, **29**, 136-154 (2012)
- 11 Nicot, F., Hadda, N., Guessasma, M., Fortin, J., & Millet, O.: On the definition of the stress tensor in  
12 granular media. *International Journal of Solids and Structures*, **50**(14-15), 2508-2517 (2013).
- 13 Nicot, F., Xiong, H., Wautier, A., Lerbet, J., Darve, F.: Force chain collapse as grains column buckling  
14 in granular materials. *Granul. Matter*, **19**(2) (2017)
- 15 Nicot, F., Kruyt, N. P., Millet, O.: On Hill's lemma in continuum mechanics. *Acta Mechanica*, **228**(2),  
16 1581–1596 (2017)
- 17 Nguyen, N. S., Magoaric, H., Cambou, B., & Danescu, A. Analysis of structure and strain at the meso-  
18 scale in 2D granular materials. *International journal of solids and structures*, **46**(17), 3257-3271  
19 (2009)
- 20 Nguyen, N. S., Magoaric, H., Cambou, B.: Local stress analysis in granular materials at a meso-scale.  
21 *Int. J. Numer. Anal. Methods Geomech.*, **36**(14), 1609-1635 (2012)
- 22 Nguyen, H.N.G., Prunier, F., Djeran-Maigre, I., Nicot, F.: Kinetic energy and collapse of granular  
23 materials. *Granul. Matter*, **18**(1) (2016)
- 24 Nguyen, N. S., Magoaric, H., Vincens, E., Cambou, B.: On the definition of a relevant meso-scale for  
25 upscaling the mechanical behavior of 3D granular materials. *Granul. Matter*, **22**(1), 25 (2020)
- 26 Nguyen, S. K., Magoaric, H., Vincens, E., & Cambou, B. Towards a new approach for modeling the  
27 behavior of granular materials: A mesoscopic-macroscopic change of scale. *International Journal of  
28 Solids and Structures*, **97**, 256-274 (2016).
- 29 Marteau, E., Andrade, J. E.: A model for decoding the life cycle of granular avalanches in a rotating  
30 drum. *Acta Geotechnica*, **13**(3), 549-555 (2018)
- 31 Méjean, S., Faug, T., Einav, I.: Discrete Element Method simulations of standing jumps in granular  
32 flows down inclines. In EPJ Web of Conferences, EDP Sciences, **140**, 03026 (2017)
- 33 Peng, C., Guo, X., Wu, W., Wang, Y.: Unified modelling of granular media with smoothed particle  
34 hydrodynamics. *Acta Geotechnica*, **11**(6), 1231-1247 (2016)
- 35 Peters, J. F., Muthuswamy, M., Wibowo, J., Tordesillas, A.: Characterization of force chains in granular  
36 material. *Physical Review E*, **72**(4), 041307(2005)



1 Radjai, F., Jean, M., Moreau, J. J., Roux, S.: Force distributions in dense two-dimensional granular  
2 systems. *Physical Review Letters*, **77**(2), 274 (1996)

3 Sibille, L., Villard, P., Darve, F., Aboul Hosn, R.: Quantitative prediction of discrete element models on  
4 complex loading paths. *Int. J. Numer. Anal. Methods Geomech.*, **43**(5), 858-887 (2019)

5 Šmilauer, V., et al.: Yade reference documentation. *Yade Documentation*, **474**(1) (2010)

6 Staron, L., Vilotte, J. P., Radjai, F.: Preavalanche instabilities in a granular pile. *Physical Review Letters*,  
7 **89**(20), 204302 (2002)

8 Staron, L., Radjai, F., Vilotte, J. P.: Multi-scale analysis of the stress state in a granular slope in transition  
9 to failure. *The European Physical Journal E*, **18**(3), 311-320 (2005)

10 Tordesillas, A.: Force chain buckling, unjamming transitions and shear banding in dense granular  
11 assemblies. *Philosophical Magazine*, **87**(32), 4987-5016 (2007)

12 Vescovi, D., Berzi, D., di Prisco, C.: Fluid–solid transition in unsteady, homogeneous, granular shear  
13 flows. *Granul. Matter*, **20**(2), 27 (2018)

14 Walker, D. M., Tordesillas, A., Froyland, G. Mesoscale and macroscale kinetic energy fluxes from  
15 granular fabric evolution. *Physical Review E*, **89**(3), 032205 (2014)

16 Wan, R., Nicot, F., Darve, F.: *Failure in Geomaterials – A Contemporary Treatise*. ISTE Press – Elsevier  
17 (2017)

18 Wautier, A., Bonelli, S., Nicot, F.: Scale separation between grain detachment and grain transport in  
19 granular media subjected to an internal flow. *Granul. Matter*, **19**(2), 22 (2017)

20 Wautier, A., Bonelli, S., Nicot, F.: Micro-inertia origin of instabilities in granular materials. *Int. J. Numer.*  
21 *Anal. Methods Geomech.*, **42**(9), 1037-1056 (2018a)

22 Wautier, A., Bonelli, S., Nicot, F.: Flow impact on granular force chains and induced instability. *Physical*  
23 *Review E*, **98**(4), 042909 (2018b)

24 Welker P., McNamara S.: Precursors of failure and weakening in a biaxial test. *Granul. Matter*, **13**, 93-  
25 105 (2011)

26 Yan, B., & Regueiro, R. A.: Definition and symmetry of averaged stress tensor in granular media and  
27 its 3D DEM inspection under static and dynamic conditions. *International Journal of Solids and*  
28 *Structures*, **161**, 243-266 (2019).

29 Zhu, H., Nicot, F., Darve, F.: Meso-structure evolution in a 2D granular material during biaxial loading.  
30 *Granul. Matter*, **18**(1), 3 (2016)

31

1

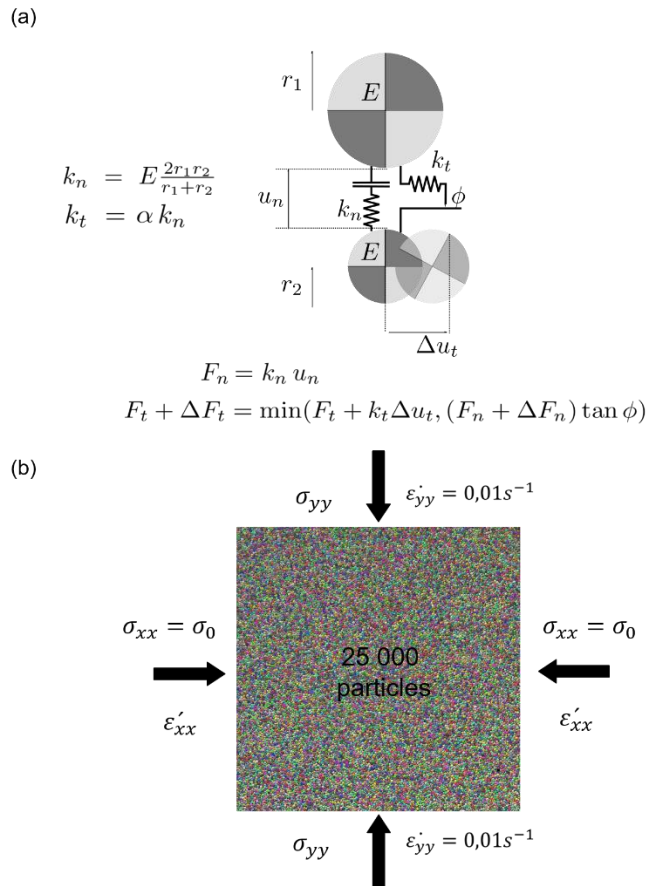
2 Table 1. Parameters of the numerical simulation.

Grain density	3000 kg/m <sup>3</sup>
Friction coefficient $\mu$	0.7
$k_n/D$	356 MPa
$k_t/k_n$	0.42
Loading rate $\dot{\epsilon}$	0.01 s <sup>-1</sup>
Numerical damping coefficient	0.05
$D_{max}/D_{min}$	3.5
Confining stress $\sigma_0$	100 kPa

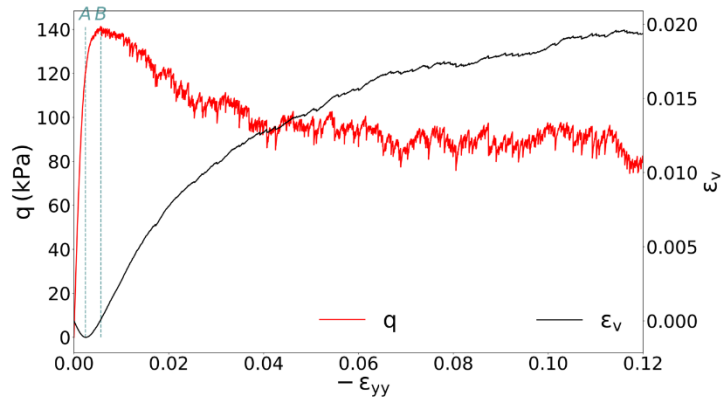
3

4

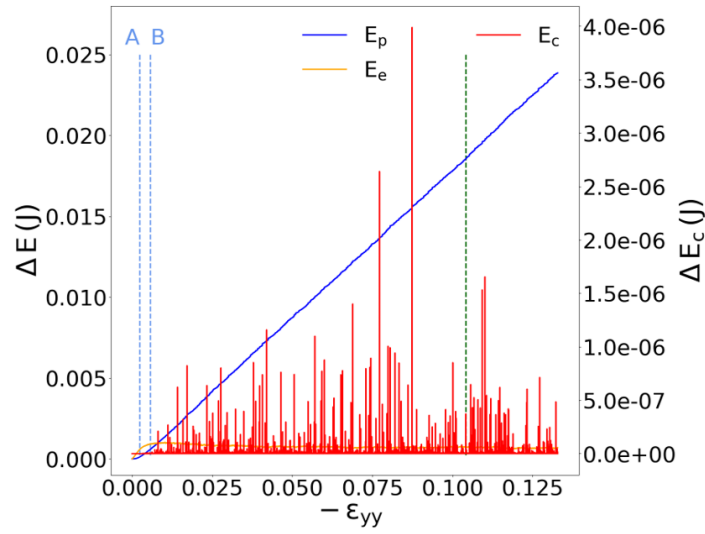
5



- 1 Figure 1. (a) Contact law used in discrete element method. The sketch shows the definition of the
- 2 stiffness coefficients and how the different components of the force contact are calculated.
- 3 (b) Drained biaxial test: representation of the quasi 2D dense sample of 25,000 spheres and loading
- 4 conditions.
- 5

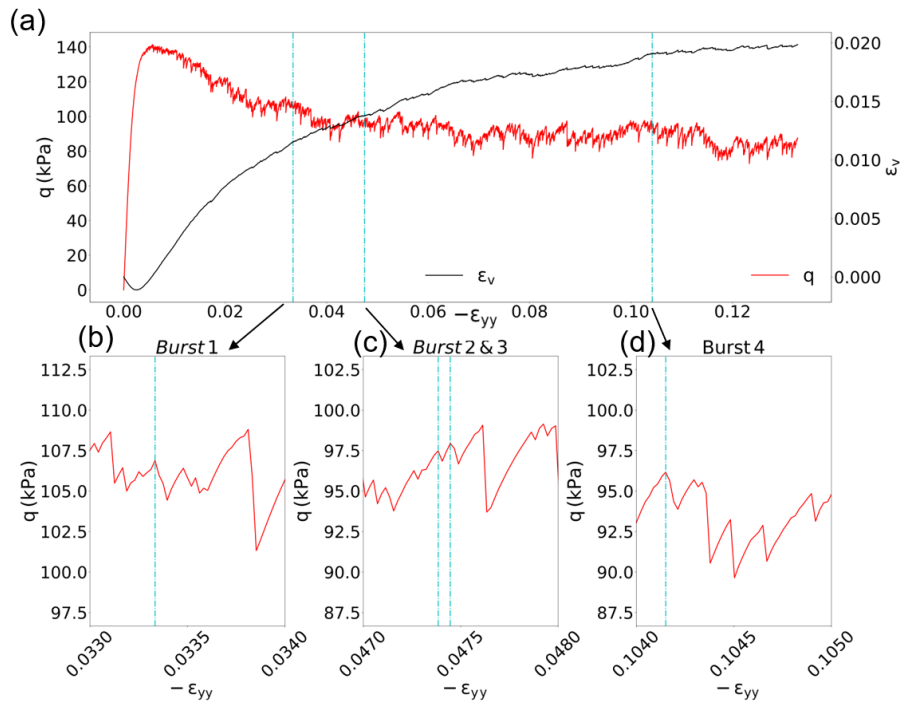


- 6
- 7 Figure 2. Deviatoric stress and volumetric strain as a function of the axial strain during the biaxial test.
- 8



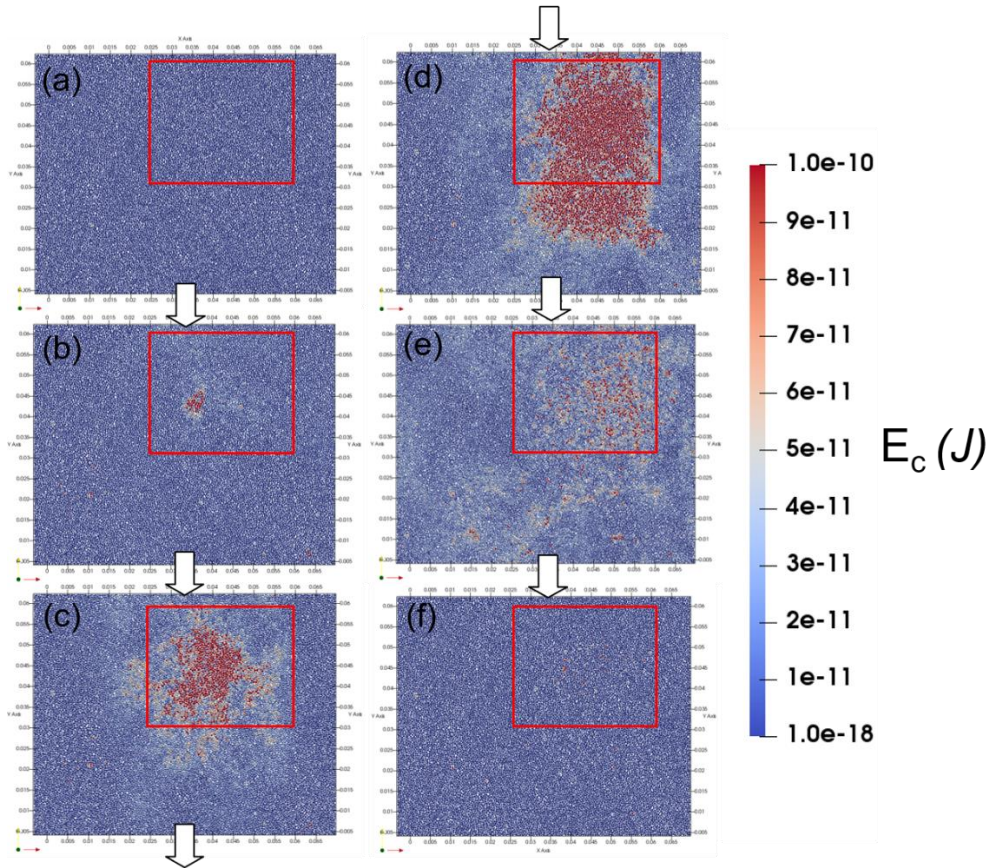
1  
2  
3  
4  
5  
6  
7

Figure 3. Evolution of elastic energy  $E_e$ , plastic dissipation  $E_p$  (left y-axis) and kinetic energy  $E_c$  (right y-axis) as a function of the axial strain during the biaxial test. The reference state corresponds to the isotropic compression state reached before the deviatoric loading is applied. State A and B correspond to the characteristic and the peak points shown in Figure 2. The burst of kinetic energy analysed in this paper corresponds to  $-\varepsilon_{yy} = 0.104$  (green dashed line).



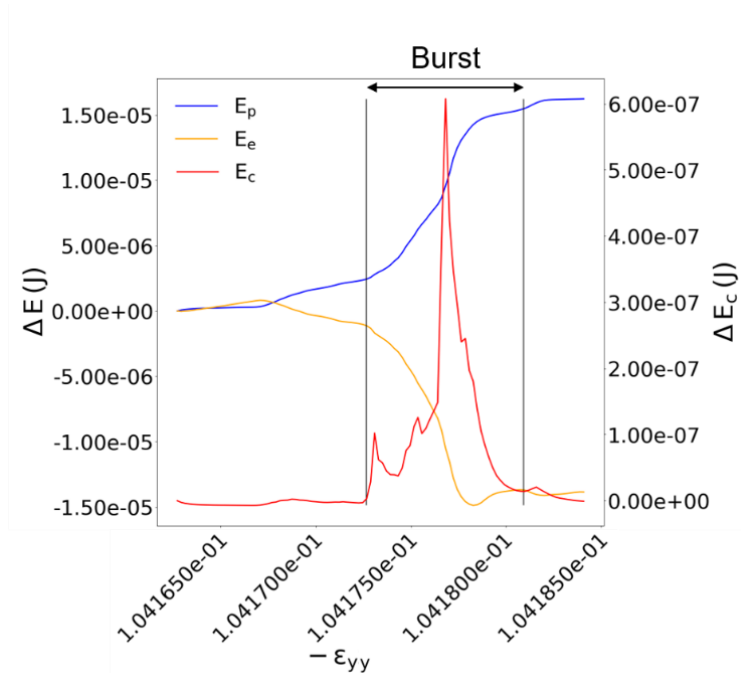
8  
9  
10  
11

Figure 4. Analysis of the four bursts considered in the manuscript, in terms of deviatoric stress  $q$  evolution during the biaxial test. The vertical lines correspond to the beginning of bursts.



1  
2  
3  
4  
5  
6

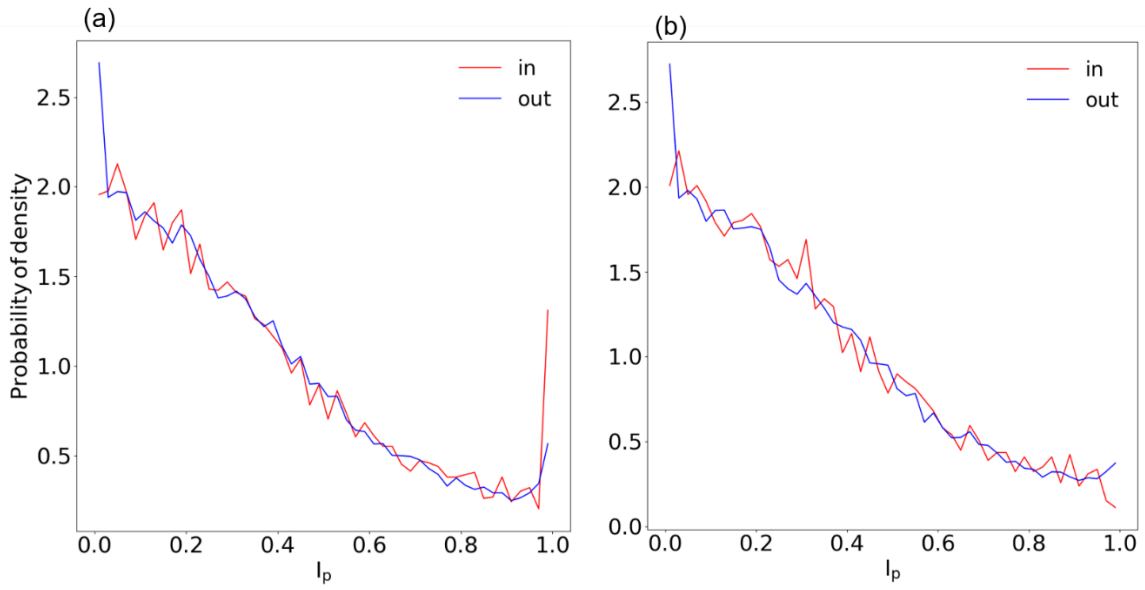
Figure 5. Reduced time lapse of the burst of kinetic energy No.4. Particles are coloured according to their kinetic energy (in Joule). The bounding box used to provide an approximate definition of the burst domain is shown in red.



7  
8  
9

Figure 6. Evolution of the plastic dissipation  $E_p$ , of the elastic energy  $E_e$  (left y-axis), and of the kinetic energy  $E_c$  (right y-axis) during the burst of kinetic energy No. 4.

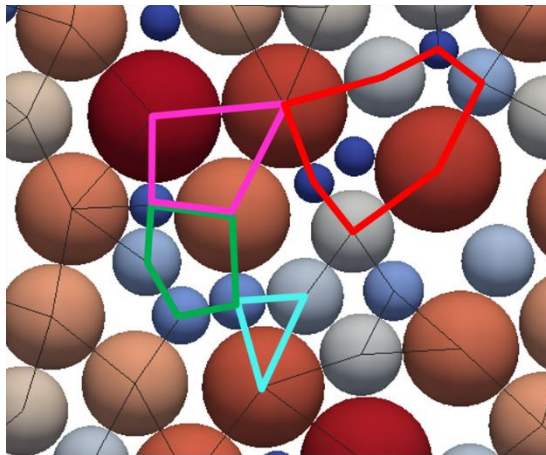
1



2

3 Figure 7. Sliding index's probability density before (a) and after (b) the burst of kinetic energy inside  
 4 (red) and outside (blue) the surroundings of the burst area.

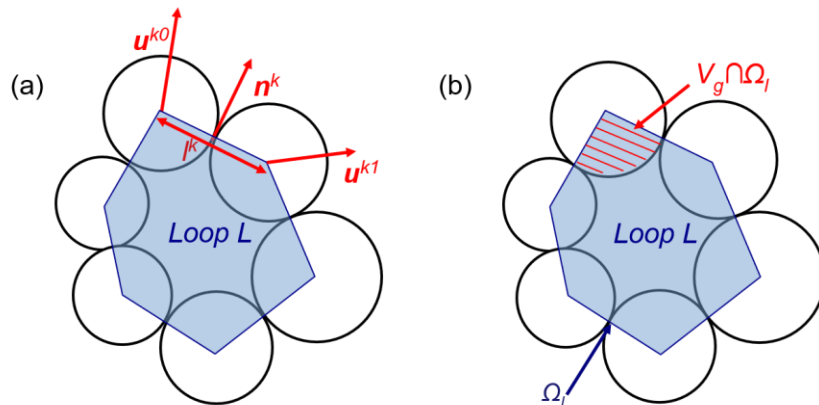
5



6

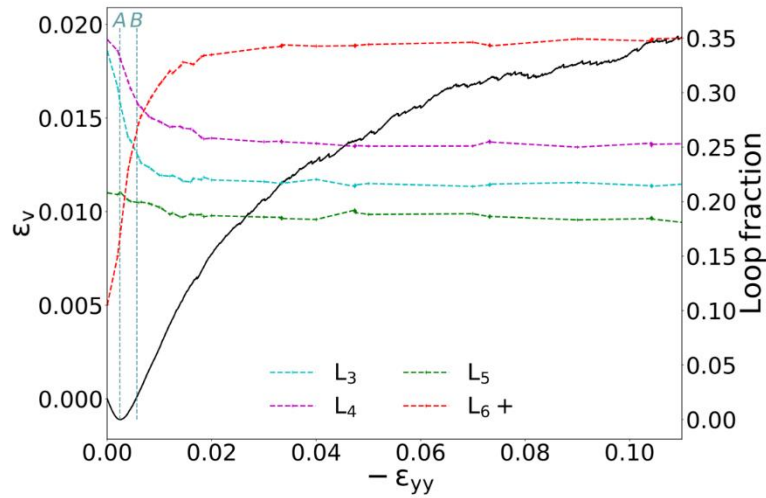
7 Figure 8. Insight of the tessellation of the sample domain into loops. Focus on four loops of different  
 8 order (L3, L4, L5 and L6).

9



1 Figure 9. Sketch of the calculation of the strain (a) and stress (b) defined at the scale of a meso-  
 2 domain.

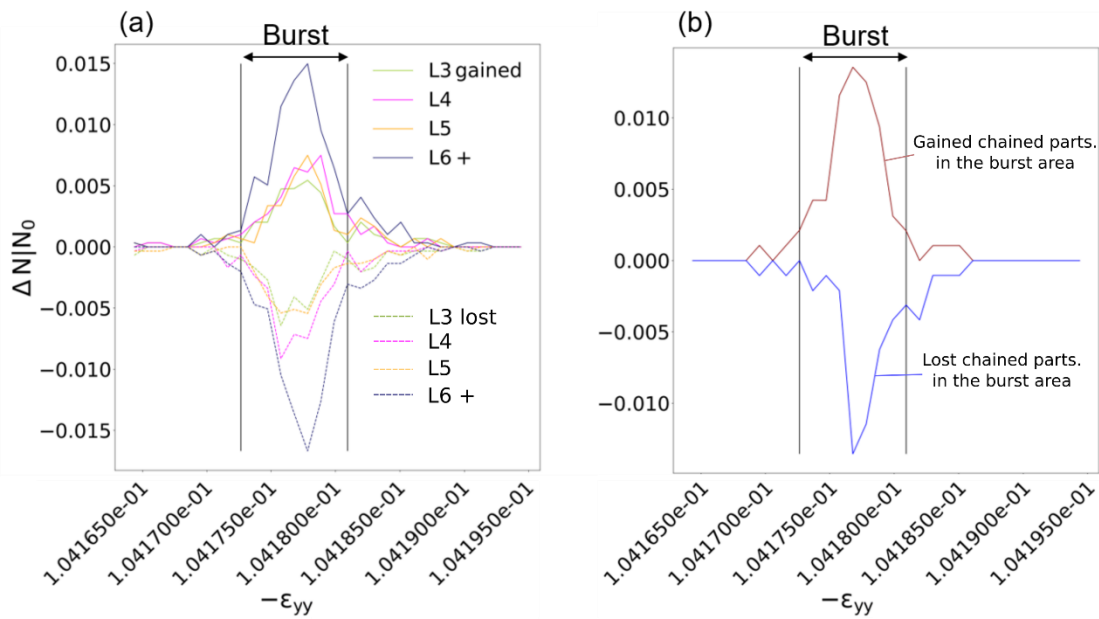
3



4

5 Figure 10. Evolution of loop fractions as a function of the axial strain during the biaxial test. The  
 6 macroscopic volumetric strain is recalled in black. The characteristic point (A) and stress peak (B)  
 7 defined in Figure 2 are shown with vertical dashed lines.

8

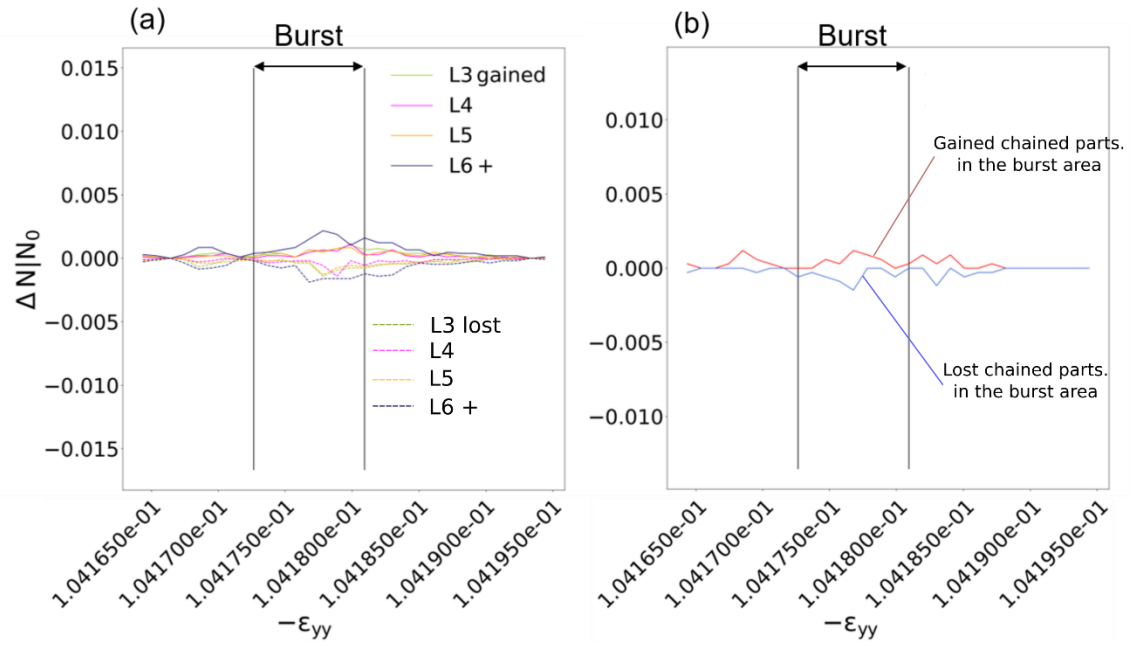


9

10

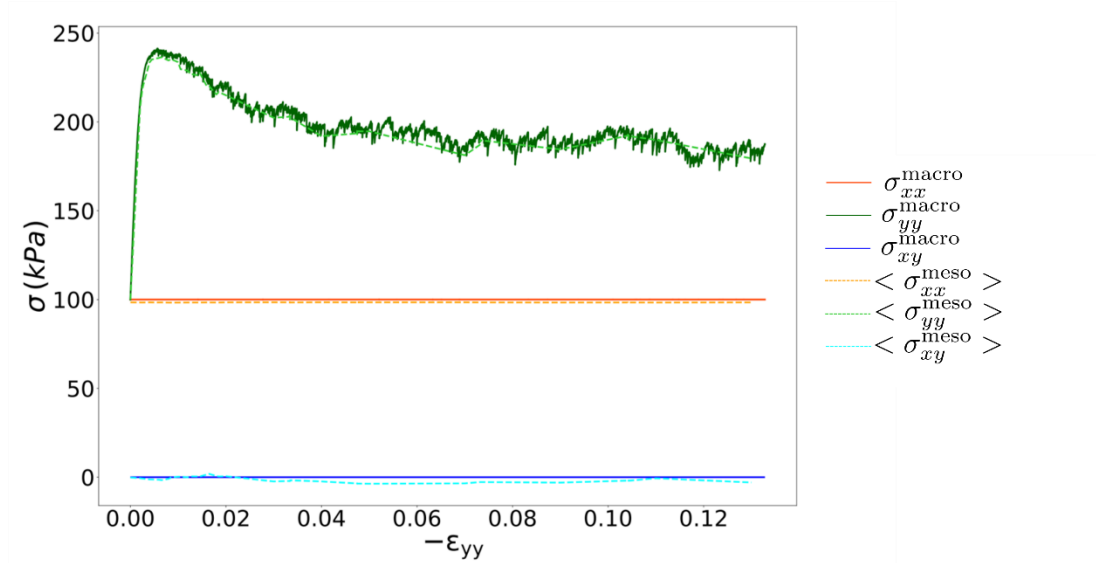
11 Figure 11. Relative variation of grain loops (a) and rattlers (b) in the bounding box domain shown in  
 12 Figure 5 (in the vicinity of the burst of kinetic energy).

13



1  
2  
3  
4  
5  
6

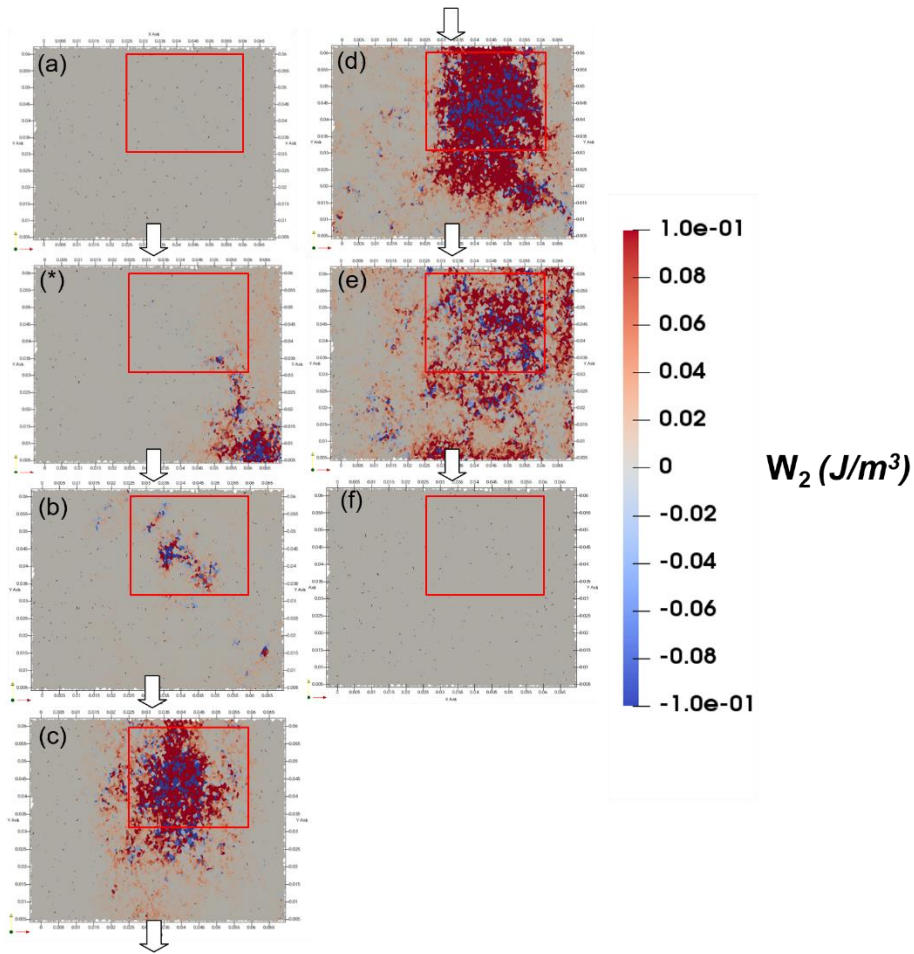
Figure 12. Relative variation of grain loops (a) and rattlers (b) outside the bounding box domain shown in Figure 5 (far from the burst of kinetic energy).



7  
8  
9  
10  
11

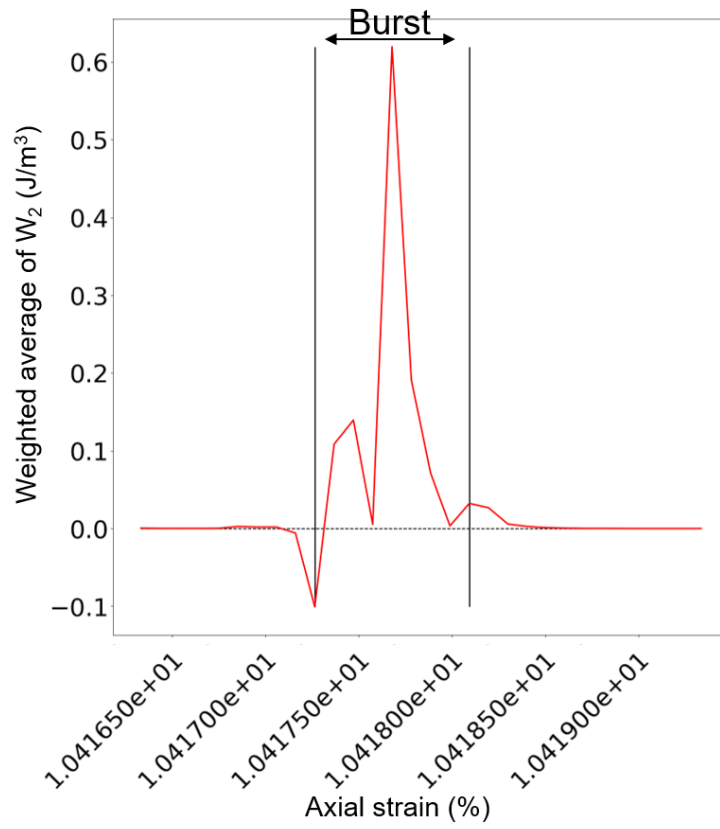
Figure 13. Comparison between the macroscopic stress  $\sigma^{macro}$  and the volume average of the mesoscopic stress  $\langle \sigma^{meso} \rangle$ .





1  
2  
3  
4  
5  
6  
7  
8

Figure 14. Reduced time sequence of mesoscopic second-order work ( $W_2$  based on the Figure 7. (a) (b) (c) (d) (e) (f) correspond to the same step of Figure 7 while (\*) corresponds to an additional step between (a) and (b). A macroscopic axial strain increment  $|\varepsilon_{yy}| = 10^{-6}$  is used to compute the incremental meso-strains and meso-stresses. The box delimiting the burst shown in Figure 5 is reproduced here.



1

2 Figure 15. Volume weighted average of the second-order work during the burst of energy, in the  
3 neighbour of the initiation of the burst.

4